Molecular Vision 2016; 22:1137-1155 <http://www.molvis.org/molvis/v22/1137>
Received 18 May 2016 | Accepted 23 September 2016 | Published 26 September 2016

Citrullination of glial intermediate filaments is an early response in retinal injury

John W. Wizeman,[1] Anthony P. Nicholas,[2] Akihito Ishigami,[3] Royce Mohan[1]

[1]Department of Neuroscience, University of Connecticut Health Center, Farmington, CT; [2]Department of Neurology, University of Alabama at Birmingham and the Birmingham VA Medical Center, Birmingham, AL; [3]Molecular Regulation of Aging, Tokyo Metropolitan Institute of Gerontology, Tokyo, Japan

Purpose: A hallmark of retinal gliosis is the increased detection and modification of the type III intermediate filament (IF) proteins vimentin and glial fibrillary acidic protein (GFAP). Here, we investigated vimentin and GFAP in Müller glia in a mouse model of alkali injury, focusing on the posttranslational modification of citrullination.

Methods: Mice were injured by corneal exposure to 1.0 N NaOH, and eyes were enucleated at different time points following injury. The levels of soluble and cytoskeletal forms of IF proteins and citrullination were measured using western blot analysis. Citrullinated GFAP was identified by immunoprecipitation followed by two-dimensional (2D) isoelectric focusing–polyacrylamide gel electrophoresis (IEF-PAGE) western blotting using a specific antibody that recognizes citrullinated GFAP. Vimentin, GFAP, and citrullinated proteins were localized in the retina by immunohistochemistry (IHC). Drug treatments were investigated in retinal explant cultures of posterior eyecups obtained from mouse eyes that were injured in vivo.

Results: Detection of GFAP in injured retinas increased over a period of 1 to 7 days, showing increased levels in both soluble and cytoskeletal forms of this IF protein. The global level of citrullinated proteins was also induced over this period, with low-salt buffer extraction showing the most abundant early changes in citrullination. Using IHC, we found that GFAP filaments assembled at Müller glial end feet, growing in size with time through the inner layers of the retina at 1–3 h postinjury. Interestingly, over this early time period, levels of soluble citrullinated proteins also increased within the retina, as detected by western blotting, coincident with the localization of the citrullinated epitopes on growing GFAP filaments and existing vimentin filaments by 3 h after injury. Taking advantage of the in vivo injury model to promote a robust gliotic response, posterior eyecups from 7-day postinjured eyes were treated in explant cultures with the peptidyl arginine deiminase inhibitor Cl−amidine, which was found to reduce global citrullination. Surprisingly, the detection of injury-induced high-molecular-weight GFAP species containing citrullinated epitopes was also reduced by Cl−amidine treatment. Using a low dose of the potent type III IF drug withaferin A (WFA), we showed that Cl−amidine treatment in combination with WFA reduced global protein citrullination further, suggesting that GFAP may be a key component of pathological citrullinated targets.

Conclusions: Our findings illuminate citrullination as a potential novel target for trauma-induced retinal gliosis. We also propose that strategies for combining drugs targeting type III IFs and citrullination may potentiate tissue repair, which is an idea that needs to be validated in vivo.

Gliosis is a pervasive and complex process that occurs in many central nervous system (CNS) disorders and after traumatic injury, where astroglial cells become reactive, proliferate, and undergo hypertrophy [1,2]. A major hallmark of reactive gliosis is the overabundance of the type III intermediate filament (IF) proteins vimentin and glial fibrillary acidic protein (GFAP). When stimulated by stress signals or injury, radial Müller glia, which span the entire width of the retina, initiate reactive gliosis by increasing levels of GFAP. Soluble tetrameric precursors of GFAP, along with vimentin, copolymerize into long filamentous forms that create an elaborate cytoskeleton network [3]. Notably, heightened detection of GFAP and vimentin filaments has been found in several major human retinal diseases [4-6]. As such, the pathological overabundance of GFAP and vimentin in Müller glia can drive the formation of scar tissue [7,8].

Scar tissue exerts tractional forces on retinal membranes, distorting underlying vital cellular structures; to remedy this, surgery is currently the only treatment option [9]. Corroborating such a pathological role for overabundance of type III IFs in neurodegeneration, the deficiency of vimentin and GFAP in mice is protective in several stress-related and injury contexts [1,10]; however, the tissue fragility due to the complete lack of filaments underscores the importance of these type III IFs in the normal structural function of Müller glia [11]. The ability to regulate glial reactivity to promote wound healing and halt destructive aspects of glial

Correspondence to: Royce Mohan, Department of Neuroscience, University of Connecticut Health Center, 263 Farmington Ave, Farmington, CT 06030-3401; Phone: (860) 679 2020; email: mohan@uchc.edu

overactivation could benefit from a greater understanding of how vimentin and GFAP are regulated during the injury-repair process.

Vimentin and GFAP are both regulated by multiple posttranslational modifications (PTMs) [12-17]. These PTMs include citrullination, also known as deimination. Citrullination is the calcium-dependent transformation of arginine residues on proteins. This reaction is performed by the enzyme family called peptidyl–arginine deiminases (PADs). There are five known PAD isoforms in the mammalian genome, PAD1 to 4 and PAD6 [18]. Citrullinated GFAP and vimentin have been observed in the brains of Alzheimer's patients [19], while citrullinated GFAP is found to accumulate in the brains of multiple sclerosis (MS) patients [20]. In the experimental autoimmune encephalomyelitis (EAE) model of MS, a small molecule inhibitor of PAD activity was able to rescue diseased mice from clinical EAE [21]. Increased citrullination has also been recently reported in the retinas and optic cups of age-related macular degeneration (AMD) donor tissues [22], as well as in glaucomatous optic nerves [23] and astrocytes exposed to increased ocular pressure [24]. While there have been several recent advancements in treatments for CNS injury [25-29], the use of PAD inhibitors has only recently been explored in an experimental model of neurotrauma [30]. In that study, effective early downregulation of protein citrullination within hours of injury that was shown to be protective highlights the importance of molecular events that occur during the early hours following CNS injury [30]. Previous studies have suggested that citrullination may affect the formation of filaments by blocking phosphorylation sites or inducing the collapse of insoluble, filamentous type III IFs [14,31]. The in vitro investigation of these type III IFs has provided the insight that citrullination affects the type III IF polymerization/depolymerization steps; however, the physiological relevance of this PTM of type III IF proteins in retinal gliosis remains unknown.

Using an alkali injury model, we previously showed that the small molecule withaferin A (WFA) targets vimentin and GFAP in Müller glia during retinal gliosis in vivo [32,33]. WFA targets type III IFs via binding to a highly conserved rod 2B domain that is common to this class of IF proteins [32,34-36]. Given its potent effects in targeting soluble forms of IFs, WFA reduces the proliferative response of Müller glial cells in gliosis, and ultimately, it also perturbs the filament structure of IFs [37]. Here, we have exploited the alkali injury model to investigate whether citrullination occurs during retinal gliosis. We show for the first time that citrullinated modified forms of vimentin and GFAP filaments are detected extremely early after injury. Using the alkali-injured mouse eyes in an explant culture model [32], we also establish that this system can robustly enhance citrullination ex vivo, providing a convenient method to investigate the signaling axis that links reactive gliosis with citrullination using pharmacological inhibitors of citrullination and type III IFs.

METHODS

Ethics statement: All animal experiments were conducted in accordance with procedures approved by IACUC committee of the University of Connecticut Health Center. Mice were housed in specific pathogen–free cages in designated laboratory animal housing facilities.

Drug treatments in retinal explant culture system: N-α-benzoyl-N5-(2-chloro-1-iminoethyl)-L-Orn amide (Cl–amidine) was purchased from EMD Millipore (#506282, Billerica, MA). WFA was purchased from Chromadex (Santa Ana, CA).

Mice and ocular injuries: 129S6/SvEVTac mice were purchased from Taconic (Hudson, NY) and bred in house. Over 100 mice of approximately 2–3 months of age were used in this study. Corneal alkali injuries were performed in 129S6/SvEVTac (Taconic) mice of either sex, as previously described [32], with a minor modification. Mice were given an intraperitoneal (i.p.) injection of ketamine/xylazine, and corneas were anesthetized with proparacaine eye drops. A 1-µl drop of 1N sodium hydroxide was then applied directly to the central cornea for 45 s. The 1N alkali strength is widely used in experimental mouse models [38] and has clinical relevance [39]. Following injury, the eye was immediately flushed extensively with sterile PBS solution (2.9 mM sodium phosphate dibasic, 1.06 mM potassium phosphate monobasic and 155 mM sodium chloride, pH 7.4; Cat # 10010-023, Gibco, Waltham, MA). The corneal epithelium was gently removed using a Tooke knife, and eyes were then treated topically with atropine (1% ophthalmic solution, Bausch & Lomb, Rochester, NY) followed by tobramycin (0.3% ophthalmic solution, Bausch & Lomb, Rochester, NY) and erythromycin (0.5% ophthalmic paste, Bausch & Lomb, Rochester, NY). For time-course studies, injured mice were treated daily with topical applications of tobramycin and erythromycin for 3 days postinjury and humanely sacrificed by CO_2 inhalation at different times. Equal numbers of male and female mice were pooled in the experiments, and all mice underwent bilateral alkali injury.

Retinal dissections: Mice were sacrificed by CO_2 asphyxiation followed by cervical dislocation and eyes enucleated immediately, and placed into sterile ice-cold PBS containing antibiotic/antimycotic (A/A) solution (Cat # 15240-062, Gibco, Waltham, MA) until dissection on ice [32].

Posterior eyecup explant culture: Enucleated eyes from mice at 7 days postinjury were dissected under sterile conditions to separate the posterior eyecup from the anterior aspect. The posterior eyecups containing the neural retina, RPE, choroid, and sclera [32] were briefly rinsed in PBS, and then one eyecup was distributed per well into 750 µl DMEM/F12 (Dulbecco's Modified Eagle Medium/Nutrient Mixture F-12; Cat # 11965-092, Gibco, Waltham, MA) medium + A/A (Invitrogen, Waltham, MA) solution and 10% fetal bovine serum (FBS; Atlanta Biologicals, Flowery Branch, GA) in a 24-well culture dish. The eyecups were placed in a 5% CO_2 incubator at 37 °C and subject to drug treatments. Fresh batches of either Cl−amidine or WFA were replenished daily for a treatment period of 3 days in DMEM cell culture medium containing 10% FBS or left untreated. Dimethyl sulfoxide (DMSO) was used as the vehicle in similar pilot experiments related to Cl−amidine concentration studies to identify an effective concentration for treatments.

Protein extraction from retinal samples: Three mouse eyecups were placed in ice-cold soluble buffer (20 mM Tris buffer, 200 mM NaCl, 1% NP-40) supplemented with a proteinase inhibitor cocktail (Roche, Indianapolis, IN), and tissue was minced into pieces on ice. Samples were left on ice for 45 min and then spun at 20,817 ×*g* for 5 min at 4 °C. The supernatant was removed and labeled as the "soluble" fraction (containing soluble forms of IF proteins), while the pellet was placed into 1:3 diluted β-mercaptoethanol:Laemmli buffer to extract cytoskeletal forms of Ifs; it was then spun down at 20,817 ×*g* for 5 min at 4 °C. This protein extract was labeled as the "insoluble" cytoskeletal fraction. Both soluble and insoluble fractions were then passed repeatedly through a 26-gauge needle 10 times to shear DNA.

Immunostaining: Unfixed eyes were first frozen in optimum cutting temperature compound (OCT; Tissue-Tek, Radnor, PA) at −80 °C before being cut on a cryostat at −24 °C. Sections were cut at a thickness of 10 or 15 µm, attached to Superfrost slides, and stored at −80 °C until used. Slides were air dried for 30 min and then fixed in ice-cold methanol/acetone (5 min/1 min). Fixed slides were washed in PBS three times for 5 min, and then primary antibody was added in Dako background reducing solution (Dako, Glostrup, Denmark) at the specified concentration. Slides were incubated with primary antibody for 3 h at 37 °C and then either washed directly or moved to 4 °C overnight for further incubation, followed by washing five times for 10 min. Slides were then incubated with secondary antibodies at specified concentrations overnight (15 h) at room temperature in the dark and subsequently washed five times for 10 min before imaging.

Western blotting: The Bicinchoninic Acid Assay (Pierce, Waltham, MA) was used for quantification of protein. Protein samples were boiled 95–100 °C for 5–10 min in Laemmli buffer and then loaded on 4–20% Tris-HCl sodium dodecyl sulfate (SDS) polyacrylamide gels (Bio-Rad, Hercules, CA). Proteins were transferred onto a 0.2 µm polyvinylidene difluoride (PVDF membrane, Bio-Rad). Membranes were blocked in 5% milk in 1X Tris-buffered saline + Tween (TBST) for 1 h at room temperature; they were then incubated with primary antibody for 1 h at room temperature or overnight at 4 °C. Membranes were washed three times for 15 min, then incubated with secondary antibody for 45–60 min at room temperature. Membranes were washed four times for 15 min and developed with enhanced chemiluminescence (ECL; Bio-Rad) solution. To normalize for protein loading, membranes were stripped in 10X Tris-glycine-SDS buffer for 30 min at room temperature (RT), then probed as above with either glyceraldehyde 3-phosphate dehydrogenase (GAPDH) or β-actin antibodies. All figures are shown with corresponding GAPDH or β-actin control beneath.

Antibodies: Primary antibodies used in the experiments for western blotting (WB) and immunohistochemistry (IHC) were as follows: rabbit polyclonal anti-GFAP (Abcam, Cambridge UK, 7779 1:4,000 WB, 1:500 IHC; Abcam 7260 1:20,000 WB, 1:500 IHC), mouse–immunoglobulin M (IgM) monoclonal F95 (anti-peptidyl-citrulline antibody, Millipore, MABN328, 1:500 WB 1:200 IHC), rabbit polyclonal GAPDH (Santa Cruz, Dallas, TX, sc25778 1:500 WB), rabbit polyclonal vimentin (Abcam, ab45939 1:200 IHC), mouse monoclonal β-actin (Sigma, St. Louis, MO A5441 1:1,000 WB), mouse β-tubulin (Santa Cruz, sc55529 1:1,000 WB), and citrullinated GFAP [40] (CTGF-1221, 1:1,000). Secondary antibodies were Santa Cruz goat anti-rabbit IgG horseradish peroxidase (HRP; sc-2301 1:1,000 WB), goat anti-mouse IgG HRP (sc-2302 1:1,000 WB), goat anti-mouse IgM HRP (Jackson ImmunoResearch, West Grove, PA, #115–035–075 1:5,000 WB), goat anti-mouse IgM 488 (Invitrogen, A21042 1:500 IHC), goat anti-rabbit IgG 488 (Invitrogen, A11008 1:500 IHC), and goat anti-rabbit IgG 594 (Invitrogen A11012 1:500).

Immunoprecipitation and two-dimensional polyacrylamide gel electrophoresis separation: Citrullinated proteins were immunoprecipitated using the F95 antibody via protein L agarose bead chromatography. In brief, on day 1, 500 µl of protein L agarose beads (Sigma-Aldrich) were washed two times for 5 min and once for 30 min in soluble buffer with phenylmethylsulfonyl fluoride (PMSF, 1 mM), NaF (5 mM), Na_3VO_4 (1 mM), protease inhibitor cocktail, and dithiothreitol (DTT, 1 mM). Following this washing step, the final

volume of protein L beads was brought to 500 µl with this soluble buffer. F95 antibody was added at 1:50 and incubated with washed protein L beads overnight on a rotator at 4 °C. On day 2, this bead–antibody mixture was spun down at 3,000 ×*g* for 2 min. This mixture was then washed two times for 5 min in soluble buffer at half concentration (10 mM Tris, 100 mM NaCl, 0.5% NP-40, 0.5 mM PMSF, 2.5 mM NaF, 0.5 mM Na_3VO_4 0.5 mM DTT) and once for 30 min; it was spun down at 3000 ×*g* for 2 min between washes. Posterior eyecups from eight injured and eight uninjured eyes were separately solubilized in 120 µl each of the original soluble buffer and treated as soluble protein. Once extracted, 100 µl of the soluble fraction of protein was added to the bead–antibody mixture, and the half concentration of soluble buffer was added to the 500-µl final volume. This mixture was then incubated on a rotator overnight at 4 °C. On day 3, this bead–antibody–sample mixture was spun down at 3,000 ×*g* for 2 min. Supernatant from this spin was removed. Beads were washed with the half concentration of soluble buffer four times for 5 min. After the final wash, soluble buffer was added to final volume of 500 µl. Following this, 400 µl of the mixture was spun down at 3,000 ×*g* for 2 min, and supernatant was removed. This bead mixture was resuspended in 160 µl reconstitution buffer (8 M urea, 2% CHAPS (3-[(3-Cholamidopropyl)dimethylammonio]-1-Propanesulfonate (CHAPS), 50 mM DTT, 0.2% Bio-Lyte 3/10 ampholytes, and Bromophenol Blue; ReadyPrep 2D Starter Kit, Bio-Rad, cat #163–2105). Samples were then heated to 95–100 °C for 10 min. After boiling, the sample was spun down for 1 min at 20,817 ×*g*. Supernatant was considered the "bound" fraction.

After immunoprecipitation, 160 µl of bound fractions were added to pH 4-7 immobilized pH gradient (IPG) strips (Bio-Rad #163–2015) and subjected to passive rehydration for 1 h followed by active rehydration at 50 V for 14 h in Bio-Rad Protean IEF Cell (Bio-Rad #165–4000). After rehydration, the IPG strips underwent isoelectric focusing following the manufacturer's instructions (Bio-Rad #163–2105). IPG strips were then run on a 4–20% gradient polyacrylamide gel (Bio-Rad #567–1091). Following polyacrylamide gel electrophoresis (PAGE) separation, the protein was transferred to a PVDF membrane, and the blots were blocked in 5% milk in 1X TBST and probed with primary antibodies as described (Western blot section). Uninjured and injured samples from the same experiment were run in parallel.

Confocal microscopy: Immunofluorescent images were taken on a confocal microscope (Zeiss LSM 780, Zeiss, Oberkochen, Germany) on individual planes isolated from xyz stacks of retinal sections with a thickness of 15 µm. Final images were four-frame averages taken at 20X or 63X magnification that were acquired randomly from retinal sections. Laser intensity was maintained across all images.

Statistical analysis: Each sample for western blot analysis contained pooled protein extracts from three separate mouse eyes, and all of the injury experiments were repeated three times to obtain quantitative results. Data represented were the mean of three experiments ($n = 3$) normalized to GAPDH or β-actin. The data were analyzed to obtain the means ± standard deviation (SD) using *t* tests, with a difference of $p<0.05$ considered statistically significant.

RESULTS

Citrullination is an early injury response in the retina: We modified a previously established mild alkali injury model where induction of retinal gliosis became prominent by day 7 postinjury, as characterized by increased detection of vimentin and GFAP in Müller glia [32]. Extending our prior findings to earlier time points (days 1, 3, and 7 postinjury), we found there was a temporal increase in GFAP immunoreactivity that was produced after injury. Notably, the soluble protein extracts revealed increased levels of GFAP (Figure 1A) and vimentin (Figure 1B). We assessed injured retinal tissues to determine the time course of gliosis-associated citrullination in the retina. We found that there was an immediate induction of citrullinated protein species that were found in the soluble fraction starting at 1 day postinjury (Figure 1C). This sustained induction of citrullination lasted until day 7. In comparison, citrullinated species in the soluble fraction of proteins were extremely low in the uninjured eye (Figure 1C, lane 1). By day 1 after injury, citrullinated proteins were visualized at a variety of molecular weights, with distinct bands at 50 and 75 kDa and a pattern of high-molecular-weight bands between 150 and 250 kDa. Overall, the increased citrullination of proteins in the soluble extracts closely paralleled the increase in the major 50 kDa GFAP protein species and its several lower-molecular-weight cleaved forms [33] produced over this period (Figure 1C ~75 kDa, arrowhead; ~50 kDa, asterisk). The distribution of citrullinated proteins within the high-molecular-weight range in the soluble fraction was also altered over the time course of injury, with a 250-kDa band increasing over time, while the 200- and 150-kDa bands leveled off between days 3 and 7 postinjury.

When we assessed the insoluble fraction of retinal lysates using the F95 monoclonal antibody, multiple bands reactive for citrullinated proteins were also present in the insoluble extracts of both injured and uninjured eyes (Figure 2). In particular, the presence of a 75-kDa citrullinated protein was slightly increased by 3 days after injury (Figure 2A; arrowhead, ~75 kDa). While the 50-kDa species increased early

after injury and then decreased by 7 days, the changes in this species were not significant. (Figure 2A, asterisk, ~50 kDa). In contrast, GFAP in the insoluble fraction showed an increase through 7 days (Figure 2D), while vimentin increased through 3 days and returned to the levels of uninjured eyes at 7 days (Figure 2E). Altogether, our findings showed that there were global changes in protein citrullination that occurred after injury, and these reflected a temporal progression with the early onset of retinal gliosis in this model.

Multiple isoforms of GFAP are citrullinated in the mouse retina: We next wanted to characterize the GFAP isoforms that become citrullinated after retinal injury. This proved to be a challenge for two major reasons. First, soluble tissue extracts retrieved from retinas 7 days after injury exhibit at least 28 distinct GFAP antibody–reactive spots by two-dimensional (2D) isoelectric focusing (IEF)-PAGE and western blot analysis (Appendix 1). This suggested the likelihood of a complex citrullinated GFAP pattern. Second, a recent finding showed that with increasing levels of citrullination on GFAP, its binding to the GFAP antibody is increasingly lost [40], highlighting the difficulty of identifying these modified GFAP isoforms by either F95 or GFAP immunoprecipitation. Fortunately, a novel antibody raised against citrullinated GFAP (CTGF-1221) that recognizes this PTM at positions R270 and R416 in humans (R267 and R413 in mice, respectively) was developed in that study [40]. Using immunoprecipitation, citrullinated proteins from the soluble pool of retinas at 7-day postinjury were affinity isolated using the F95 antibody and subjected to IEF-PAGE. These protein blots were then subjected to incubation with the CTGF-1221 antibody to detect citrullinated GFAP. As a comparison, soluble fractions from uninjured retinas were also analyzed by IEF-PAGE and western blotted with the CTGF-1221 antibody. The 2D immunoblots from uninjured retinas probed with the CTGF-1221 antibody did not identify reactive species (Figure 3A). In contrast, 2D immunoblots from injured retinas probed with the CTGF-1221 antibody revealed intense reactivity at the anticipated 50–52 kDa size for citrullinated GFAP species (Figure 3B). The major immunoreactive region showed two closely spaced 50–52 kDa overlapping species distributed over isoelectric points of 5.25–5.6 (Figure 3B, box). A second region between isoelectric points of 4.50–5.00 was detected, with additional minor species being detected between the two boxed regions (Figure 3B, box). These two boxed regions correspond to the ~50 kDa broad band that was observed by one-dimensional western

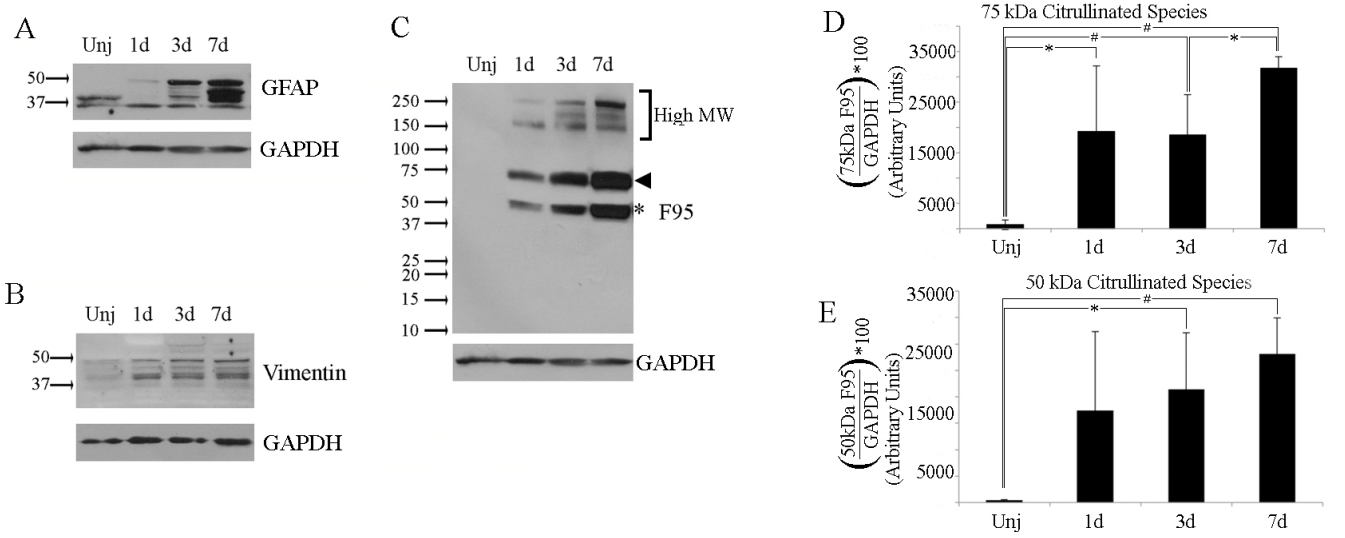

Figure 1. Detection of soluble citrullinated proteins after ocular alkali injury. Western blot analysis of soluble protein extracts from retinochoroidal tissues of uninjured eyes (lane 1) and mouse eyes injured in vivo for 1, 3, and 7 days. **A**: Blots were probed for glial fibrillary acidic protein (GFAP). **B**: Blots were probed for vimentin. **C**: Blots were probed for citrullinated proteins (F95 antibody). All blots were probed for glyceraldehyde 3-phosphate dehydrogenase (GAPDH) as a loading control. The major 50-kDa band (C, asterisk), and 75-kDa band (**C**, arrowhead), along with minor high-molecular-weight-bands over 150- to 250-kDa bands (bracket) were identified at all stages postinjury when examined for citrullination. GFAP antibody reactive species were detected between 37 kDa and 50 kDa (**A**). Uninjured and injured eyes exhibit vimentin reactivity at isoforms ranging from 37 to 55 kDa (**B**). **D**, **E**: Bar graphs represent quantification of the 75- and 50-kDa citrullinated species. Each sample contained tissue extracts pooled from three retinas from which soluble protein was extracted as described in Methods. Experiments were repeated three times (n =3). Data are expressed as the mean ± standard deviation (SD). P values less than 0.01 (hashtag) as well as less than 0.05 (asterisk) were considered significant as determined by t test.

blots with the F95 antibody (Figure 1C). To detect all of the citrullinated species, the blots were reprobed with the F95 antibody. The uninjured retinas showed broad immunoreactive diffuse spots at 75 kDa and between 37 and 50 kDa with isoelectric points of 5.5–6.0 (75 kDa, Figure 3C) and 4.5–5.75 (37–50 kDa, Figure 3C). This detection is likely due to the immunoprecipitation with F95 antibody. Similarly, the blot from injured retinas displayed F95 immunoreactivity at a range of molecular weights and isoelectric points (Figure 3D, boxed regions). Specifically, an intensely labeled broad region located around 75 kDa and less intensely labeled broad region around 50 kDa closely resembled the immunoreactive bands seen in Figure 1C (arrowhead and asterisk, respectively). The multiple 75 kDa species were distributed between isoelectric points at 4.50–5.00 and 5.25–5.75, whereas those at 50 kDa were species of low abundance and were distributed between isoelectric points at 4.50–5.00 and 5.25–5.60 (Figure 3D, boxed regions). We also identified a region between 37 kDa and 50 kDa that contained immunoreactive species between isoelectric points of 5.25 and 5.60. The protein blots of soluble extracts from retinas at 7 days postinjury probed for native GFAP (Appendix 1), when overlaid on 2D IEF western blot of extracts subjected first to F95 immunoprecipitation and then 2D separation, revealed that citrullinated GFAP species (detected by CGTF-1221 antibody) migrated differently from native GFAP species (Appendix 2). These data revealed that the injured retina retained a considerable amount of GFAP in the soluble fraction as diverse citrullinated species.

Citrullination occurs on type III IFs within Müller glia: We next investigated the spatial and temporal patterns of citrullination on injury during the early time points of tissue repair in relation to vimentin and GFAP staining. The uninjured retina displayed minimal F95 reactive species in the inner retina, while the outer plexiform layer (OPL) was absent of any staining (Figure 4A-C). Long filamentous structures and colocalization with F95 reactive species were observed in Müller glia as early as 1 h after injury (Figure 4D-F, asterisk). We observed both a punctate staining starting at the ganglion cell layer (GCL) through the inner plexiform layer (IPL) and inner nuclear layer (INL), as well as filamentous structures throughout the inner retina. Immunoreactivity was also observed in the OPL (Figure 4D-F). Interestingly, filamentous structures that were interspersed with both GFAP-positive and F95-positive regions were seen in Müller glia

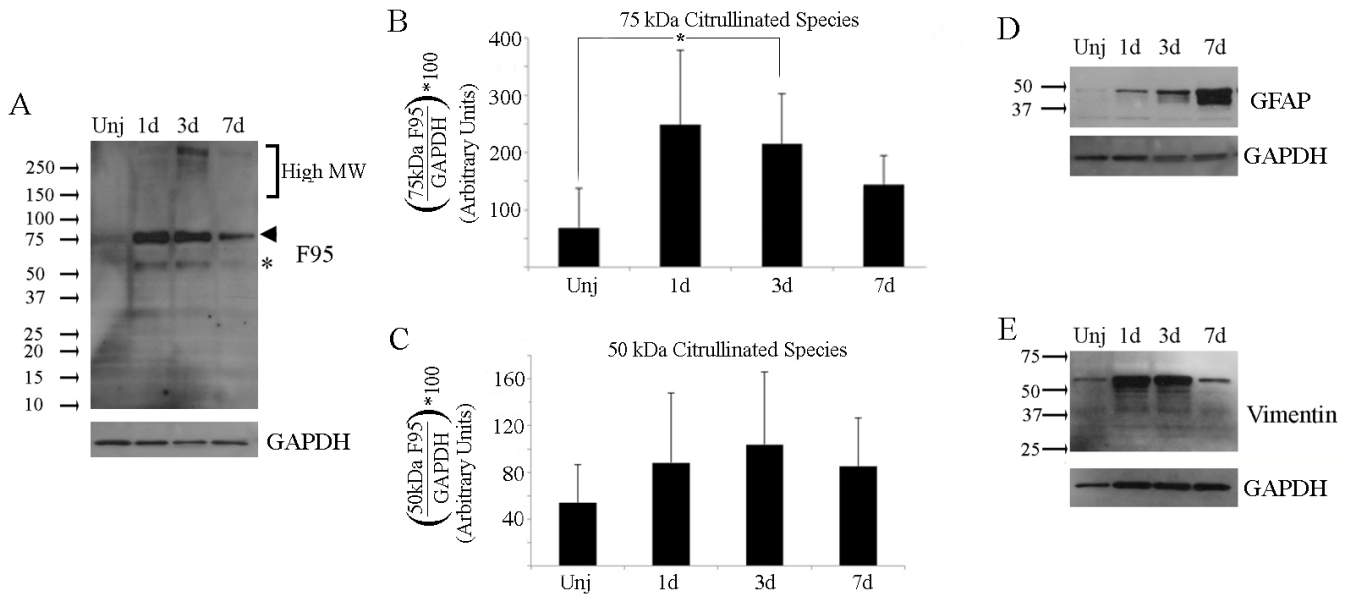

Figure 2. Detection of insoluble citrullinated proteins after ocular alkali injury. Western blot analysis of insoluble proteins from retinochoroidal tissues from uninjured and injured mouse eyes were carried out as described in Figure 1. Gel blots were probed sequentially for citrullinated proteins (F95), GFAP and vimentin. Corresponding GAPDH loading controls are located beneath each blot. **A**: Citrullinated proteins were detected in all insoluble fractions with major bands detected at 75 kDa (arrowhead) and at 50 kDa (asterisk), with minor bands over the high molecular weight range between 150 kDa and 250 kDa (bracket). **B**, **C**: Bar graphs representing quantification of the 75 and 50 kDa citrullinated species, respectively. **D**: GFAP isoforms were detectable at all time points below 37 kDa and 50 kDa. **E**: A 55 kDa vimentin isoform was detectable at all time points. Each sample contained tissue extracts pooled from 3 retinas from which protein that was not solubilized in low-salt buffer was extracted as described in Methods. Experiments were repeated three times (n=3). Data are expressed as the mean ± standard deviation (SD). P values less than 0.05 (asterisk) were considered significant as determined by t test.

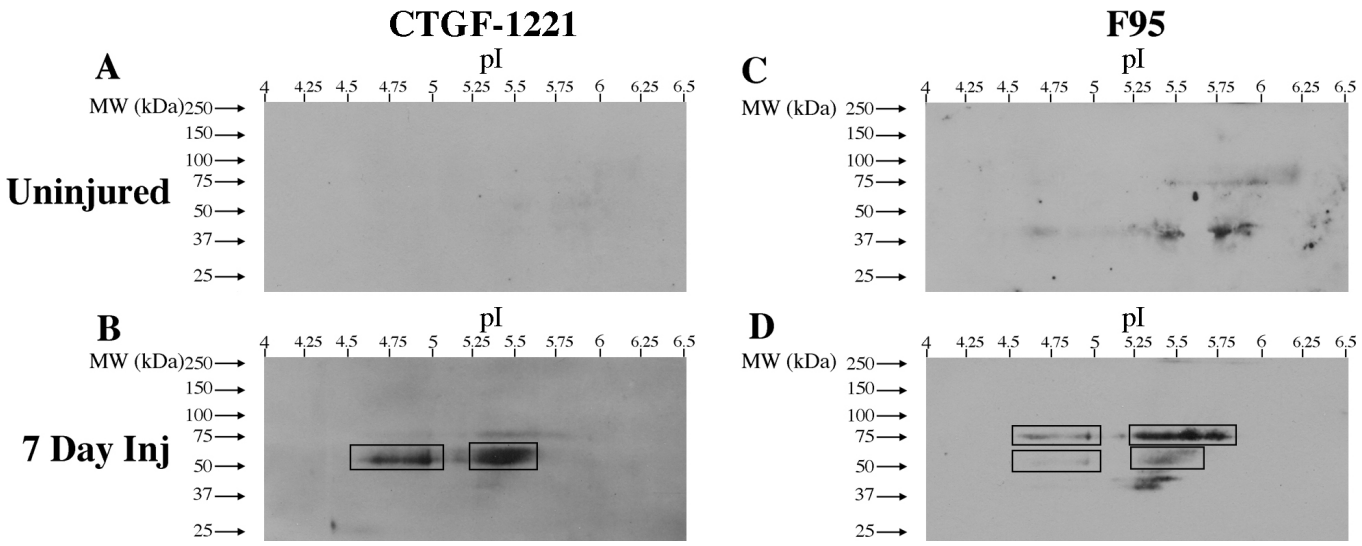

Figure 3. Detection of citrullinated GFAP in uninjured and injured retinas. The figure shows two-dimensional (2D) IEF-PAGE separation of soluble proteins from uninjured and 7 days postinjury retinochoroidal tissues immunoprecipitated for citrullinated proteins (F95 antibody) and western blotted. **A**, **B**: CTGF-1221 antibody was employed first for antigen detection. **C**, **D**: F95 antibody was subsequently employed for antigen detection after removal of CTGF-1221 antibody probe. Blots of the injured retinas probed with the anti-citrullinated GFAP antibody (**B**) showed lower relative abundance of ~50 kDa protein species compared to 75 kDa species when re-probed with F95 antibody (**D**).

at 3 h (Figure 4G-I, brackets) but not at 1 day (Figure 4J-L); they were observed again by 3 days postinjury (Figure 4M-O, brackets). These filaments were visually different from the colocalization of GFAP and F95 immunostaining and are referred to as "interspersed" filaments. These interspersed filaments showed distinct regions of F95 immunoreactivity alternating with regions of GFAP immunoreactivity along extended filamentous structures. Filaments exhibiting colocalization of GFAP and F95 persisted through 3 h after injury (Figure 4G,I asterisks), while long filament-like structures of citrullinated proteins (Figure 4H,I, arrowheads) were observed to be absent of GFAP. At 1 day after injury, there was a strong detection of F95-positive species within the INL. Noncontinuous filaments were observed extending below an enlarged astrocyte (Figure 4L, asterisk). Strong colocalization of GFAP staining with F95 immunoreactivity was observed in the GCL and IPL at 3 days after injury (Figure 4O, asterisk). Long GFAP filaments were established by 3 days after injury, and colocalization of GFAP and F95 staining occurred near the border of the GCL and IPL. With time, nuclei in the GCL displayed F95 immunoreactivity, and GFAP-positive processes extended into the vitreous, indicating a separation from the inner limiting membrane (ILM; Appendix 3). Full-length vimentin filaments (Figure 5) were observed throughout the layers of the retina in the uninjured Müller glia (Figure 5A-C), as has been previously reported [29,32]. As early as 1 h after injury, vimentin immunoreactivity within the outer layers of the retina was diminished, while colocalization with F95 reactive species was observed in the IPL (Figure 5D-F, asterisk). As with GFAP staining, filaments interspersed with both vimentin-positive regions and F95-positive regions were seen predominantly in the IPL, extending into the GCL (5F, brackets). Three hours after injury, colocalization of vimentin staining and F95 immunoreactive species was observed (Figure 5G-I, asterisk), and filaments extended beyond nuclei in the GCL into the intravitreal space (Figure 5I, arrows). One day after injury, filamentous vimentin was observed throughout the layers of the inner retina, with nuclear F95 staining (Figure 5J-L). The extension of vimentin-positive processes into the vitreous was also observed at 3 days postinjury (Figure 5O, arrow; Appendix 3). Long vimentin filaments also became interspersed with F95 immunoreactive species by 1 h (Figure 5F, brackets), into 3 h (Figure 5I, brackets), and at 3 days postinjury (Figure 5O, brackets). Müller glia recovered the full filament structure by 1 and 3 days after injury but also displayed perinuclear staining of both vimentin and citrullination in the OPL (Figure 5O, arrowhead). Of note is the border between the OPL and the INL, which displayed a strong abundance of vimentin and F95 immunoreactivity at 1 and 3 days, respectively. The rearrangement of these filaments and their citrullination highlighted the importance of examining early and immediate responses to injury.

We also examined the pattern of citrullination at higher magnification. The distinct pattern observed previously was

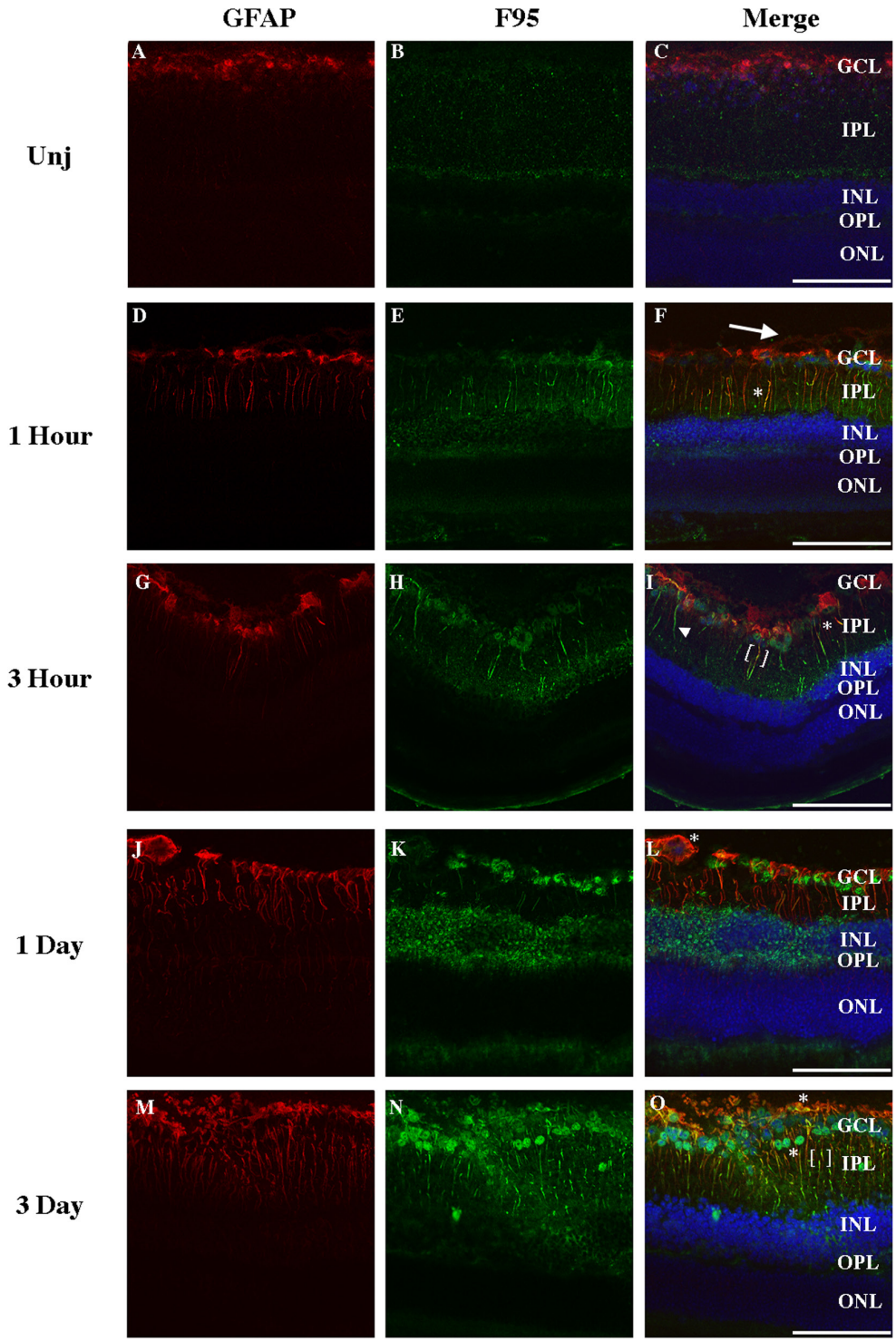

Figure 4. Citrullination of GFAP filaments after injury. Cryosections from uninjured and injured eyes were stained with GFAP (red) and F95 (green) and nuclei stained with DAPI (blue). Sections were examined under confocal microscope at 20X magnification in an uninjured state (**A**-**C**) and at 1 h (**D**-**F**), 3 h (**G**-**I**), 1 day (**J**-**L**) and 3 days (**M**-**O**) postinjury. Extensions of GFAP staining beyond nuclei of the GCL are marked by an arrow (**F**). Co-localization of GFAP and F95 antibodies are marked by asterisks (**F**, **I**, **L**, **O**). Interspersed regions of GFAP and F95 reactivity is outlined in brackets (**I**, **O**). GFAP-negative, F95-positive filaments are marked by arrowhead (**I**). GCL, ganglion cell layer; IPL, inner plexiform layer; INL, inner nuclear layer; OPL, outer plexiform layer; ONL, outer nuclear layer. (Scale bar = 100 µm).

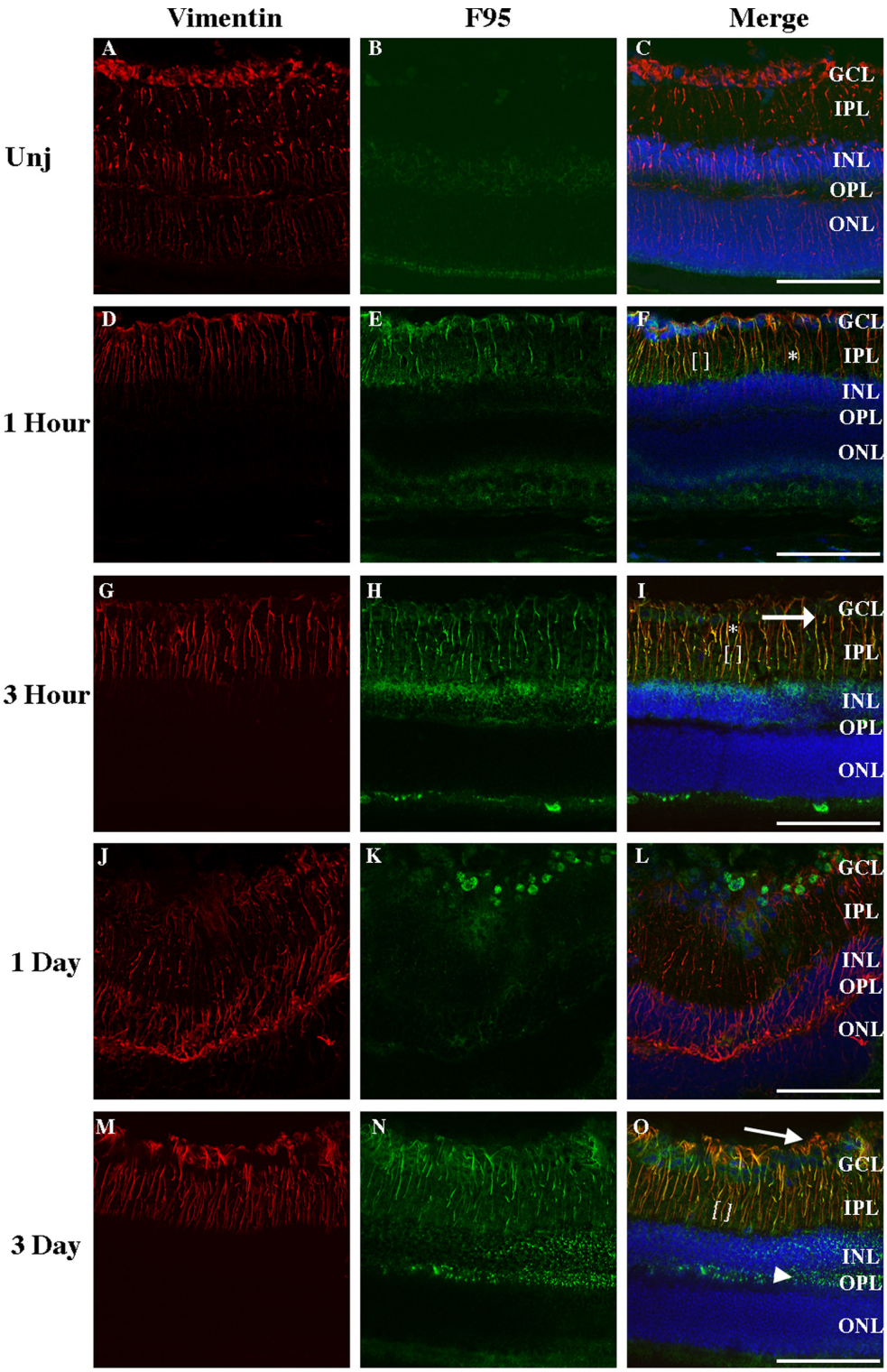

Figure 5. Citrullination along vimentin filaments after ocular injury. Cryosections from uninjured and injured eyes were stained using antibodies against vimentin (red) and citrullinated proteins (F95; green). Tissue sections were examined under confocal microscope at 20X magnification from uninjured eyes (**A-C**) and injured eyes at 1 h (**D-F**), 3 h (**G-I**), 1 day (**J-L**) and 3 days (**M-O**) postinjury. Extensions of vimentin staining beyond nuclei of GCL are marked by arrow (**I**, **O**). Representative regions showing the overlap of vimentin and F95 antibodies are marked by asterisks (**F**, **I**, **O**). Interspersed regions of vimentin and F95 reactivity are outlined in brackets (**F**, **I**, **O**). Diffuse staining of F95 is marked by an arrowhead (**O**). GCL, ganglion cell layer; IPL, inner plexiform layer; INL, inner nuclear layer; OPL, outer plexiform layer; ONL, outer nuclear layer. (Scale bar = 100 µm).

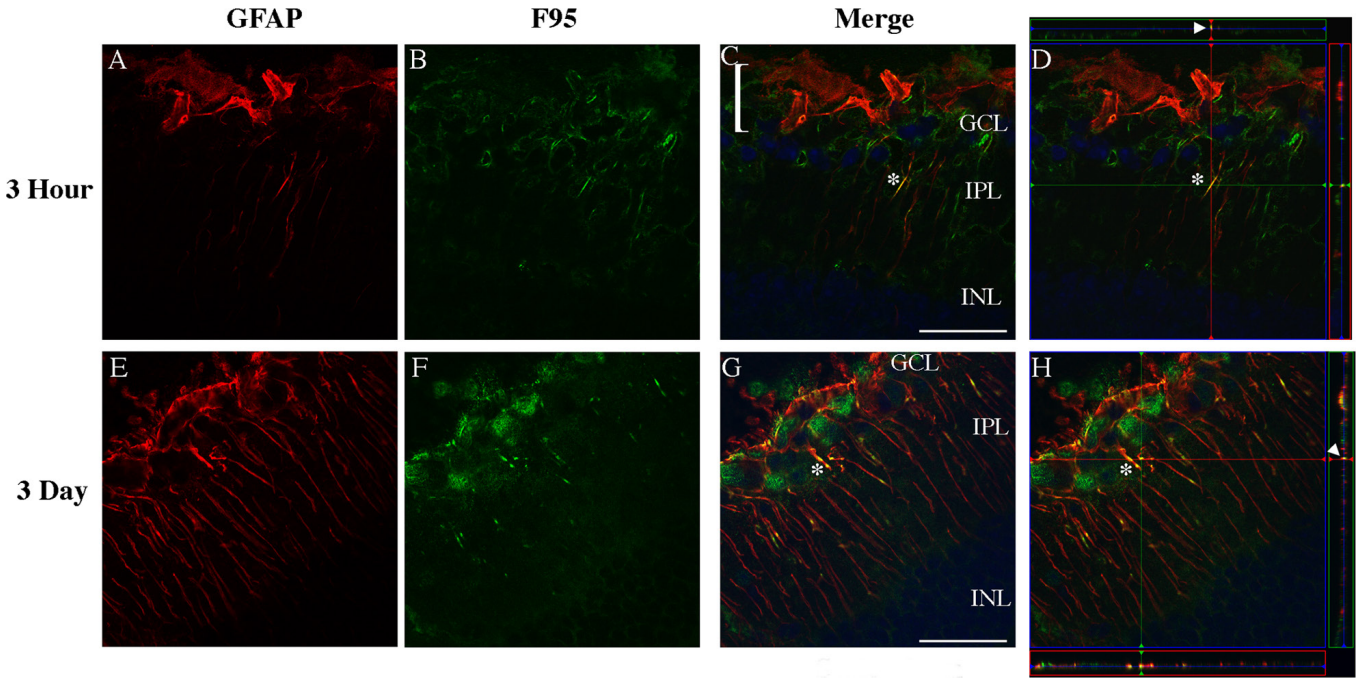

Figure 6. High magnification images of citrullinated GFAP filaments in the injured retina. Tissue sections of mouse eyes injured for either 3 h or 3 days were immunostained for GFAP (**A**, **E**, red), citrullinated proteins (**B**, **F**, F95 antibody, green), and nuclei (**C**,**G**, merged images, DAPI-blue). Sections were analyzed on a Zeiss LSM 780 confocal microscope at 63X magnification to identify GFAP filaments co-localized with citrullinated species. Colocalized filaments in 3 h (**C**, **D**, asterisk) and 3 day samples (**G**, **H**, asterisk) were visually identifiable in the inner plexiform layer (IPL). Orthogonal planes were analyzed (**D**, **H**) to identify points of co-localization (asterisks, arrowheads). Invasion of filaments into the vitreal space past the ganglion cell layer (GCL) was identified in 3 h injured samples (**C**, bracket). (Scale bar = 40 µm).

clearly visible, as both GFAP (Figure 6) and vimentin filaments (Figure 7) appeared less organized at 3 h (A-C) than at 3 days (D-F). GFAP filaments that formed at 3 h did not strongly colocalize with F95 staining (Figure 6A-D, asterisks). GFAP filaments that were extended by 3 days showed strong colocalization with F95 immunoreactivity (Figure 6E-H, asterisks). Importantly, extension of GFAP-positive processes into the vitreal space occurred as early as 3 h after injury (Figure 6C, bracket). Costaining of vimentin and citrullinated epitopes at 3 h (Figure 7A-D, asterisks) appeared to be restricted to the layers of the inner retina (GCL, IPL), while there was a distinct and clear staining of vimentin at 3 days (Figure 7E-H) in the INL and near the border between the IPL and the INL. At this later time point, F95 staining became more distinct, as glial processes stained for both vimentin and GFAP and displayed an interspersed staining with citrullinated proteins (Figure 6G, brackets), while vimentin- and GFAP-positive glial sprouts extended through the retina (Appendix 3).

Due to the changing contours of the tissue, immunostaining of Müller glia does not always provide the possibility of visualizing filaments fully. To more completely probe the nature of the IF relationship with F95 reactive species along the length of entire filaments through the contour of the retina, we compiled z stacks of confocal images into movies. Using tissue sections from the 3-h and 3-day postinjury time points, samples were stained with either GFAP and F95 or vimentin and F95. When we examined GFAP immunoreactivity at 63X magnification 3 h postinjury (Appendix 4), filaments extending into the INL were observed. When filaments were examined throughout the z-stack, both regions of "interspersed" filamentous structures and colocalized regions could be identified (Appendix 4). Several GFAP-negative, F95-positive filaments were also observed. When we examined GFAP and F95 immunoreactivity at 3 days postinjury (Appendix 5), GFAP filaments were tracked from the GCL through the INL. At 3 days, fewer GFAP-negative, F95-positive filamentous structures were observed. Regions of colocalization were observed mainly in the IPL. When examined at 3 h postinjury, vimentin immunoreactivity appeared diminished in the outer retina (Appendix 6). F95-positive, vimentin-negative filamentous structures were not observed at 3 h postinjury. Filaments predominantly displayed both F95 and vimentin immunoreactivity, with several F95 positive regions interspersed near the boundary of the IPL and the INL. At 3 days postinjury (Appendix 7), vimentin-positive

filaments were observed extending from the ONL to the GCL. F95 immunoreactivity was also observed in the INL. Vimentin and F95 immunoreactivity along the continuous filamentous structures was predominantly colocalized. An interspersed pattern was observed with vimentin and F95 immunoreactivity immediately adjacent to this pattern (Appendix 7, Figure 7G, bracket). These data indicated that citrullination in the Müller glia can associate with the IF cytoskeleton and appears to be dynamically altered as the filaments form after injury.

Targeting citrullination and the IFs in retinal gliosis reduces GFAP and vimentin: We next hypothesized that citrullination plays a role in the injury response of the retina and could impact gliosis. To test this hypothesis, we employed the PAD inhibitor Cl−amidine and exploited a retinal posterior eyecup organ culture model as a convenient biochemical assay. The retinal posterior eyecup model was previously employed to test inhibitors of gliosis in vitro using enucleated eyes from mice that had been subjected to alkali injury to promote gliosis [32]. This biochemical assay not only involves a relatively short time period to test drugs by bath application but also avoids issues with variability in tissue permeability and unknown pharmacodynamics associated with in vivo drug delivery to the retina. Thus, using the intact posterior eyecups dissected from eyes 7 days after injury, pilot experiments were performed to optimize the assay to ascertain the dose-related effects of Cl−amidine compared to vehicle; it was found that a 100 µM dose of Cl−amidine was effective in decreasing a broad range of citrullinated species (Appendix 8). We then investigated how perturbation of soluble IFs with a low dose of WFA, used alone or in combination with Cl−amidine, affected citrullination. Interestingly, we found that in addition to the anticipated 50 kDa GFAP, injured retinas also showed high-molecular-weight GFAP species (>75 kDa) in the soluble fraction (Figure 8A-B) and displayed a pattern similar to that previously documented in human CNS disease [20]. While Cl−amidine treatment alone reduced the abundance of some of the high-molecular-weight (>75 kDa) GFAP

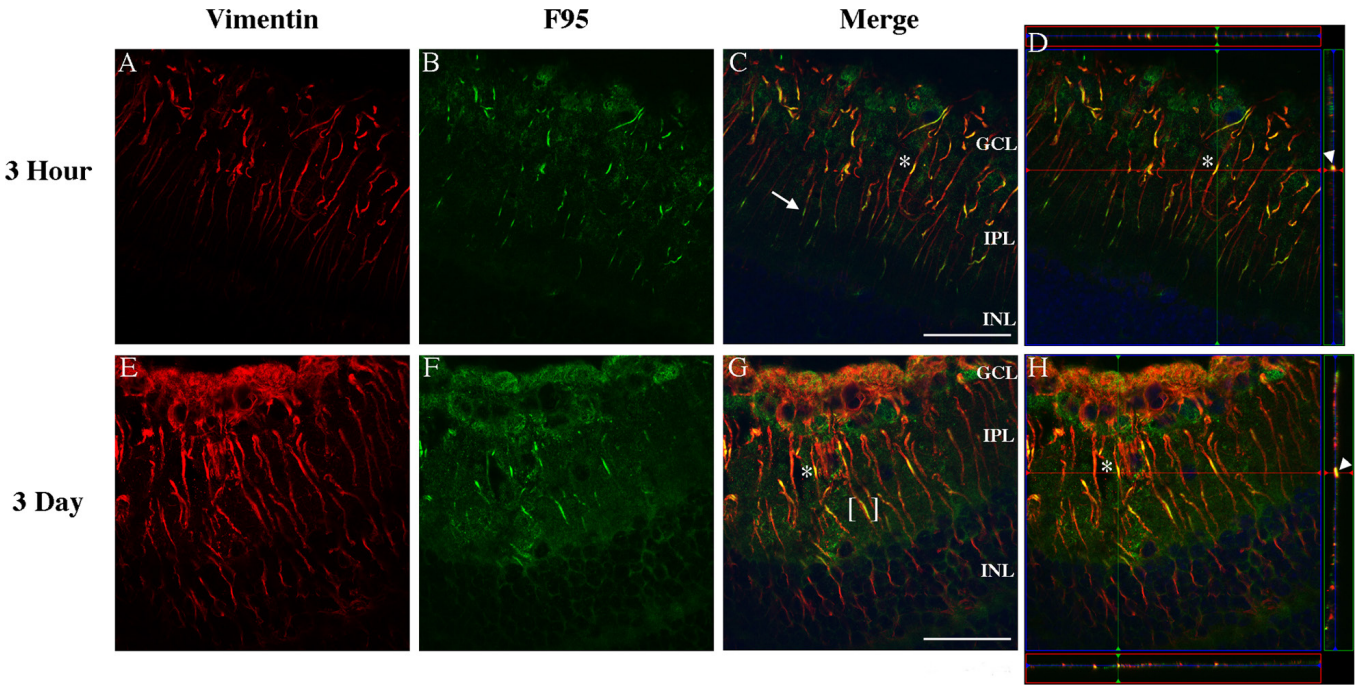

Figure 7. High magnification images of citrullinated vimentin filaments in retinas after ocular injury. Eyes injured for either 3 h or 3 days were sectioned and immunostained for vimentin (**A**, **E**, red), anti-citrullinated proteins (**B**, **F**, F95 antibody, green) and DAPI (**C**, **G**, merged images, blue). **A**: Vimentin filaments showed staining in the GCL and IPL 3 h postinjury. **B**: F95 positive filaments showed staining at 3 h post-injury in the GCL and IPL. Filaments in the retina displayed co-localization of F95 and vimentin (**C**, asterisk; **D**, asterisk/arrowhead), as well as a distinct interspersed pattern with F95 reactive regions capping filaments near the boundary of the IPL and INL (**C**, arrow). **E**: At 3 days postinjury, vimentin-positive filaments showed staining in the IPL and both filamentous and nonfilamentous vimentin immunoreactivity was present in the GCL. **F**: Diffuse staining and filamentous staining of F95 reactive proteins was present in the GCL and IPL 3 days postinjury. **G**, **H**: Vimentin and F95 displayed distinct co-localization (**G**, asterisk; **H**, asterisk, arrowhead), as well as an interspersed pattern (**G**, bracket). **D**, **H**: Orthogonal views of xyz stacks were obtained to identify points of colocalization (asterisk, arrowhead). (Scale bar = 40 µm).

species (Figure 8A), Cl−amidine in combination with WFA significantly reduced high-molecular-weight GFAP (>75 kDa) in the soluble fraction of proteins (Figure 8A). Cl−amidine also caused levels of low-molecular-weight (37–50 kDa) GFAP to be increased (Figure 8A), although the result was not statistically significant (Figure 8C). Cl−amidine treatment, however, did significantly increase the native 50 kDa GFAP species in the soluble fraction (Figure 8A, asterisk). Combined treatment with WFA and Cl−amidine increased levels of low-molecular-weight (37–50 kDa) GFAP (Figure 8A), although the result was not significant when normalized to β-actin (Figure 8C). A 55-kDa band was visibly decreased by both WFA and Cl−amidine treatment alone, and extracts from the combined treatment displayed no observable 55-kDa species (Figure 8A, arrowhead). Analysis of F95 antibody reactivity showed that treatment with both Cl−amidine and WFA clearly diminished the levels of most of the high-molecular-weight citrullinated proteins in the soluble fraction (Figure 8E). Analysis of the insoluble fraction of proteins showed no statistical difference in GFAP levels (Figure 9A-D), but changes in the migration of these species were observed (Figure 9A). Cl−amidine treatment caused a trend toward increasing abundance of the 50-kDa GFAP species, as well as low-molecular-weight GFAP (37–50 kDa) in the insoluble fraction, but these results were not significant when normalized to GAPDH (Figure 9C,D). This effect was not seen with WFA treatment alone. Taken together, our data demonstrated that when used in combination with Cl−amidine, low-dose WFA enhanced the targeting of protein citrullination and restored levels of 50-kDa soluble GFAP.

In comparison, high-molecular-weight vimentin was not readily detected in the soluble extracts (Figure 10A). Interestingly, treatment with Cl−amidine or WFA alone increased the abundance of the 55-kDa and lower species (Figure 10A, arrowhead). Combined drug treatments significantly increased the native 55-kDa vimentin species (Figure 10A,C). In contrast, the insoluble extracts did not reveal any significant changes in vimentin levels with either drug treatment (Figure 10D-F). Taken together, these biochemical experiments revealed that significant changes in the composition of the soluble pool of GFAP were affected by injury that led to increased citrullination of this IF protein, with alterations in soluble vimentin representing a minor feature of this complex reactive glial response.

DISCUSSION

We report for the first time that citrullination is an induced response to injury within Müller glial cells of the mouse retina. This PTM occurs on a global level in different cell layers of the retina, but a major citrullinated target, GFAP, and to a lesser extent, vimentin, are two important proteins of the Muller glial response to injury [1-3,6,10,11]. The discovery that the soluble form of GFAP becomes citrullinated after injury provided us with the opportunity to demonstrate that perturbation of the IFs directly by WFA [32] when combined with the pan-PAD inhibitor Cl−amidine can interfere with citrullination. Our data are intriguing, as there has been growing interest in the roles of soluble IFs, for instance, as chaperones [41] and in the nuclear transport of kinases in injured neurons and corneal fibrosis [41,42], as well as in lamellipodia formation [43,44]. Several prior studies have focused on the Müller glial responses in different injury contexts [8,28,29,32,33,45], but the immediate responses of IF proteins where soluble forms are regulated have not been studied. Also of note is that although this study focuses on glial responses and did not examine neuronal responses, retinal ganglion cells can become apoptotic after alkali injuries [46]. Our findings illuminate citrullination of IFs as an important early event in the injury response of the retina.

The citrullinated GFAP isoforms that result from this severe alkali injury showed a wide distribution of both basic and acidic species that contain the antigenic R267 or R413 citrullination sites. These data do not rule out that other arginines in GFAP could be citrullinated, as their mobilities in the 2D western blot analysis were clustered together. The presence of acidic citrullinated GFAP species, however, indicated that phosphorylation may also be contributing to the solubility of these GFAP filaments, as increased phosphorylation is known to depolymerize cytoskeletal forms of IF proteins [13,47].

Interestingly, we found that the retinal explant culturing process enhanced the extent of citrullination causing hypercitrullination, making this explant biochemical assay not only reliable but also suitable for drug testing under controlled conditions. The hypercitrullination pattern observed in cultured retinal explants appeared to be similar to that reported for human astrocytes cultured under hypoxia, where the early detection of PAD enzyme and that of a ~65 kDa GFAP citrullinated isoform were also reported [48]. That the robust hypercitrullination was observed largely in the soluble fraction, in stark contrast to the minor changes in citrullination in the insoluble fraction, indicated that the majority of citrullinated proteins in this system represent proteins that were solubilized at low-salt conditions. These data, in conjunction with the diffuse citrullinated GFAP spots seen from 2D western blots and the interrupted staining pattern of F95 in GFAP-containing filaments, suggested that that the dynamic exchange of citrullinated and phosphorylated

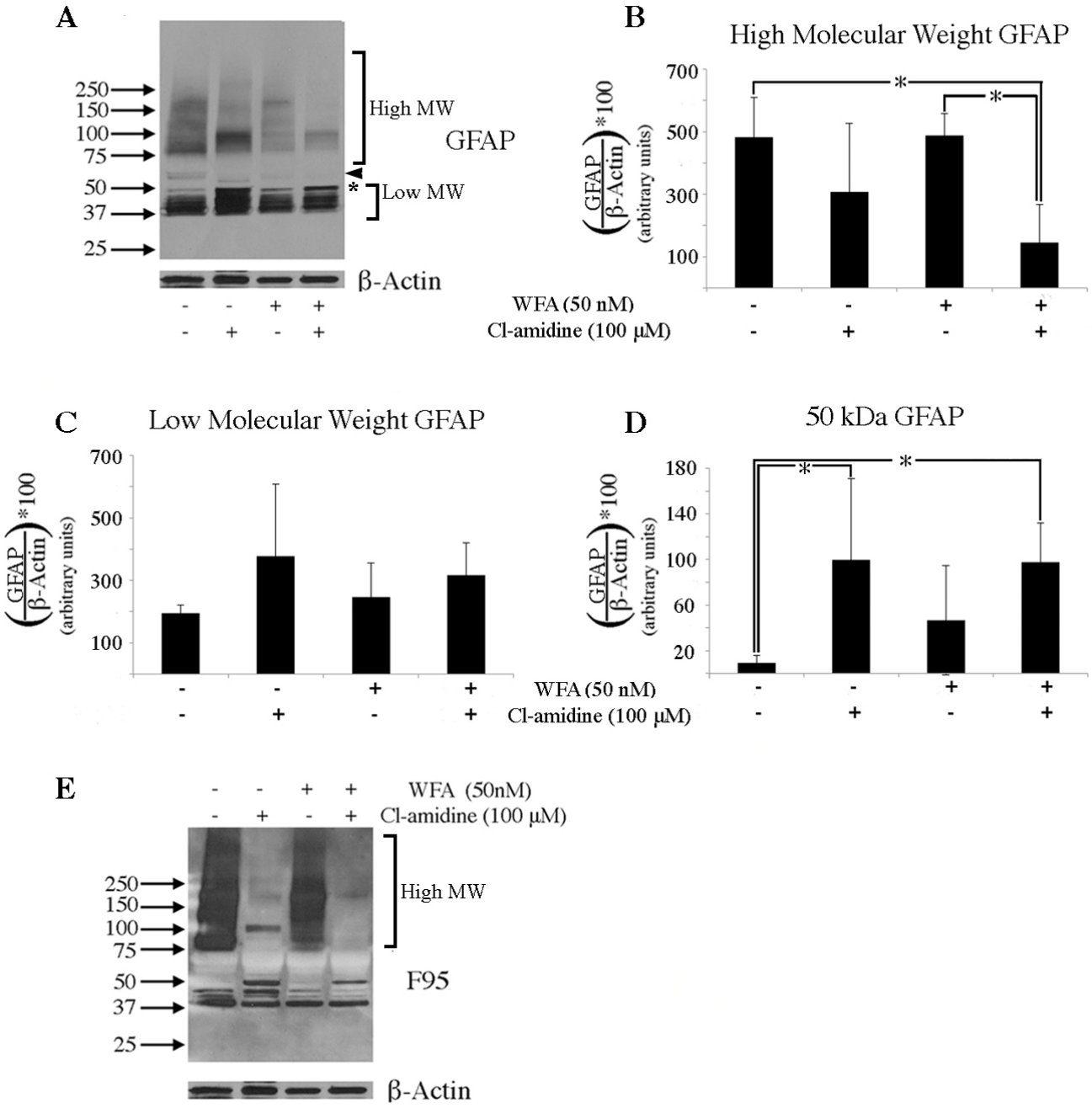

Figure 8. WFA and Cl-amidine have a compounding effect on soluble GFAP in the retina. Eyes were injured and left to recover for 7 days in vivo. On day 7, mouse eyes were enucleated and posterior eyecups were placed into culture with no drug added (lane 1), or containing either Cl-amidine alone (lane 2), WFA alone (lane 3), or both drugs combined (lane 4). **A**: Western blot analysis of GFAP in soluble fractions of untreated, Cl-amidine treated, WFA treated, or WFA/Cl-amidine treated eyecups. The arrowhead points to a 55 kDa band. Densitometric quantification of high molecular weight GFAP (**B**, >75 kDa), low molecular weight GFAP (**C**, 37-50 kDa), or 50 kDa GFAP (**D**, asterisk). **E**: Western blot analysis of F95 in soluble fraction from untreated, Cl-amidine treated, WFA treated, or WFA/Cl-amidine treated eyecups. Data are expressed as the mean ± standard deviation (SD). P values less than 0.05 (asterisk) were considered significant as determined by *t* test.

soluble GFAP with filamentous structures may be occurring during gliosis. It is possible that citrullination of vimentin may also alter antigenic reactivity, as it does with GFAP [47]. It will be important in the future to examine the citrullination patterns of both GFAP and vimentin in less severe retinal injuries that recover structural integrity to ascertain how the phenotype–biomarker relationship in retinas changes in models of reversible gliosis that promote healing over fibrosis.

Since WFA and Cl−amidine both have established targets with pathological roles that can be inhibited at nontoxic drug doses [21,32-34,37,49,50], our interest in knowing whether these drug targets interacted to affect global citrullination revealed an interesting result. Binding of WFA to soluble IFs [32], which likely causes increased IF phosphorylation [37,42], was found to increase the effectiveness of PAD inhibition when it came to inhibiting global citrullination. One explanation for the synergistic drug effect is that WFA-bound soluble GFAP may complex with active PADs, thereby sensitizing PADs to Cl−amidine. Soluble phosphorylated vimentin bound by WFA has been shown to complex with phosphorylated extracellular signal-regulated kinase-1, -2 (ERK1/2) and filamin A in myofibroblasts and to coexist in multimeric protein complexes that block nuclear translocation of pERK1/2 by WFA treatment [42]. Similarly, complexes between soluble GFAP and PADs may be induced by WFA activity that could effectively alter PAD intracellular localization or its activity through mechanisms that are as yet unknown.

The presence of IFs displaying a colocalization with citrullinated epitopes at the early stages after injury and temporal changes observed along both established and developing filaments implicate this PTM as a likely dynamic

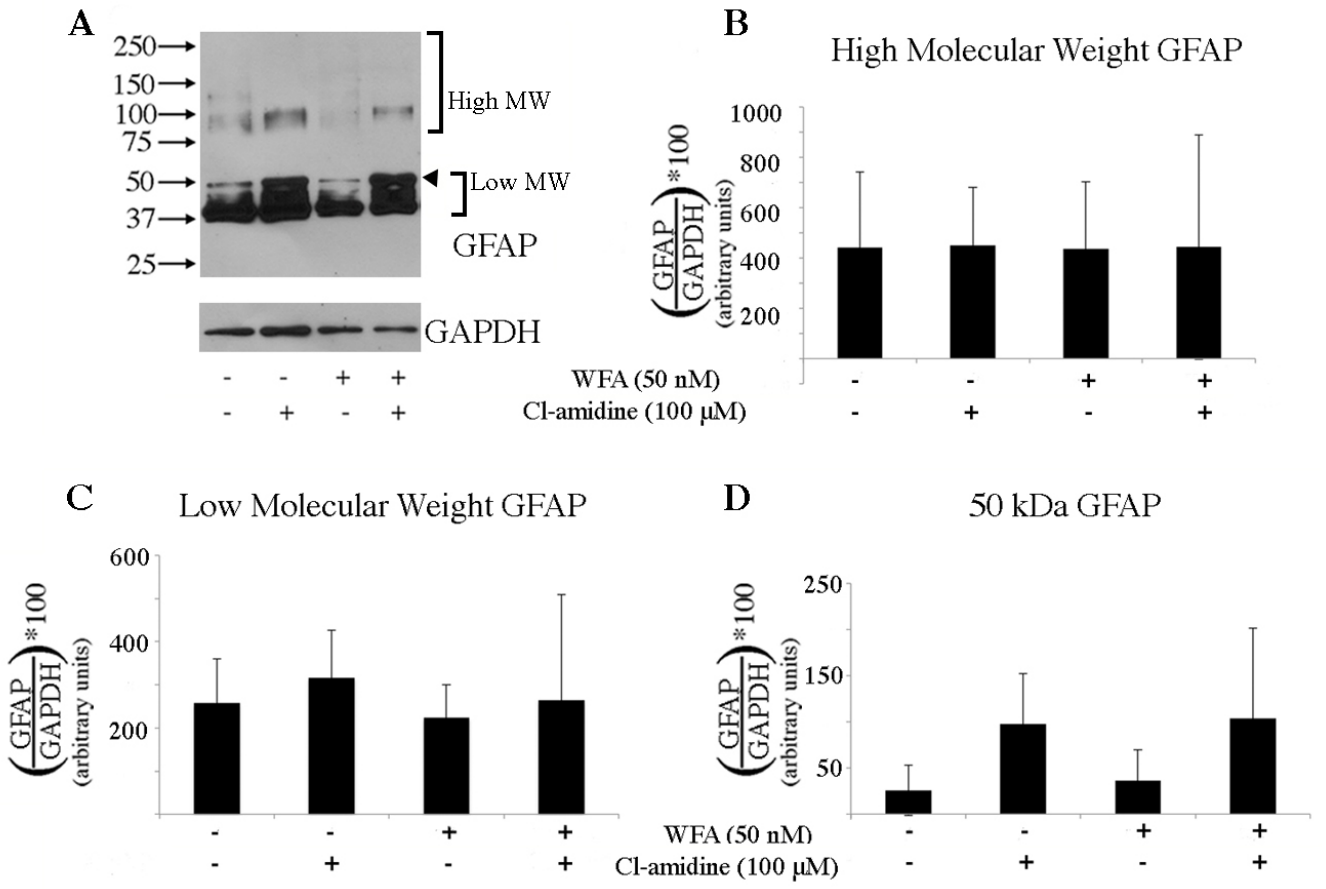

Figure 9. WFA and Cl-amidine have no effect on insoluble GFAP in the retina. Eyes were injured and left to recover for 7 days in vivo. On day 7, mouse eyes were enucleated and posterior eye-cups were placed into culture with no drug added (lane 1), or containing either Cl-amidine alone (lane 2), WFA alone (lane 3), or both drugs combined (lane 4). **A**: Western blot analysis of GFAP in insoluble fraction of untreated, Cl-amidine treated, WFA treated, or WFA/Cl-amidine treated eye-cups. Densitometric quantification of high molecular weight (**B**, >75 kDa), low molecular weight (**C**, 37-50 kDa), and 50 kDa (**D**, arrowhead) GFAP species. Data are mean ± standard deviation (SD). P values less than 0.05 were not obtained as determined by *t* test.

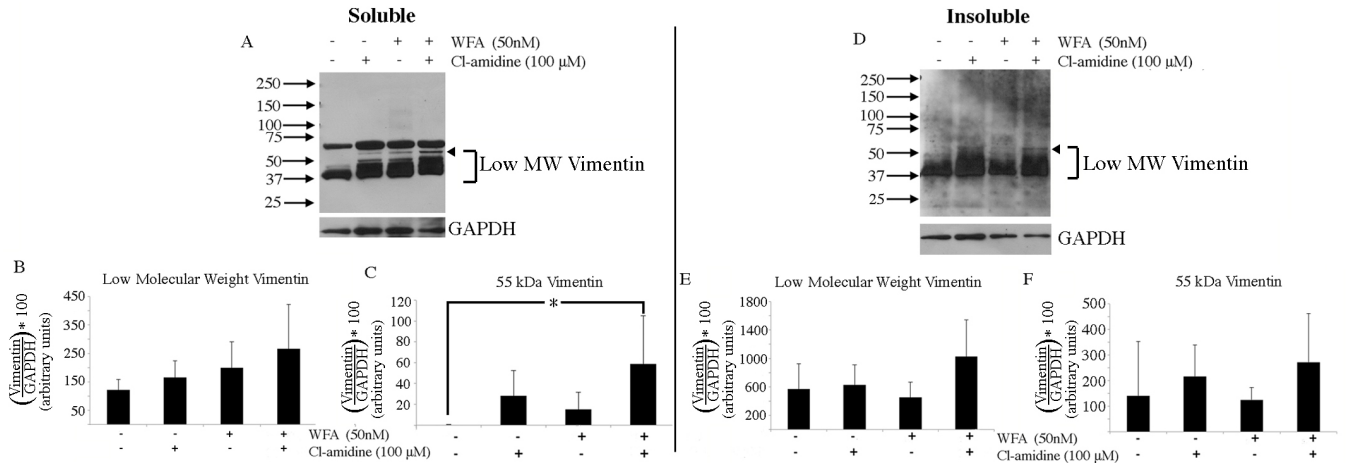

Figure 10. WFA and Cl-amidine alter the distribution of vimentin in the retina. Eyes were injured and left to recover for 7 days in vivo. On day 7, mouse eyes were enucleated and posterior eyecups (neural retina, pigment epithelium, choroid) were placed into culture containing specified concentrations of either Cl-amidine (lane 2), WFA (lane 3), both Cl-amidine and WFA (lane 4) or no drug added (lane 1). **A**: Western blot analysis of vimentin in soluble fractions of untreated, Cl-amidine treated, WFA treated, or WFA/Cl-amidine-treated eyecups. Densitometric quantification of low molecular weight vimentin (**B**, 37-55 kDa), or 55-kDa vimentin (**C**, arrowhead). **D**: Western blot analysis of vimentin in insoluble fraction of untreated, Cl-amidine treated, WFA-treated, or WFA/Cl-amidine-treated eyecups. Densitometric quantification of low molecular weight (**B**, **E**, 37-55 kDa) and 55-kDa (**C**, **F**, arrowhead) vimentin species. Data are mean ± standard deviation (SD). P values less than 0.05 (asterisk) were considered significant as determined by *t* test.

regulator of cytoskeletal alterations in Müller glia. The confocal microscopic orthogonal views highlighted this importance by showing that not only were citrullinated epitopes directly colocalized with IFs from the earliest stages but that these modifications also occurred interspersed along the length of filaments. Immunohistochemical analysis of injured retinas also showed a protrusion into the vitreal space that was reminiscent of "glial sprouts" (Appendix 3), showing some similarity to idiopathic human retinas from AMD patients [51]. These extensions into the vitreal space that are made largely from Müller glial end feet indicated a breakdown in ILM integrity. To this end, it will be important in future to examine how such changes to the IFs affect the architecture of the Müller cell.

The initial activation in injury indicates that the Müller cells, with their position near the vitreous space and the presence of stretch receptors [52], are the major glial sensors in the retina and organizers of retinal injury response. Our findings parallel those found using the laser injury model, which showed early reactivity of Müller glia preceding choroidal neovascularization, suggesting gliosis sensitizes the entire retina to retinal pigment epithelial injury [53,54]. Recent research has found that both citrullination and PAD levels were increased after exposure to increased intraocular pressure (IOP) [22-24,55]. The mouse alkali injury models the clinical outcomes of alkali injuries that are associated with glaucomatous pathology and increased IOP [56]. Müller glial cells responding to such increased IOP may be responsible for the increase in citrullination that we observed after injury and in glaucoma. While the in vivo injury maintained pressure throughout the vitreous, the explant system devoid of this increased IOP could trigger the response of Müller glia, possibly accounting for the differences seen between the in vivo injury and the explant culture system.

Despite numerous attempts to unravel the intricate responses involved in the mammalian system, gliosis has remained an untreatable condition. Here, we have identified that the PTM of citrullination is an important mechanism in reactive gliosis that could provide a druggable target for retinal disorders, as it has in other clinical conditions [57].

APPENDIX 1. TWO DIMENSIONAL IEF ANALYSIS OF GFAP FROM INJURED RETINAS.

To access the data, click or select the words "Appendix 1." Eyes from 7 day injured mouse retinas were collected and retinochoroidal tissues from the posterior eyecups were extracted into the soluble lysate. This soluble fraction was directly separated by 2-dimensional gel electrophoresis and protein blot was probed with the rabbit anti-GFAP antibody that recognizes native unmodified species.

APPENDIX 2. OVERLAID IMAGES OF GFAP AND CITRULLINATED GFAP.

To access the data, click or select the words "Appendix 2." Mouse eyes were injured and left to recover for 7 days in vivo. On day 7, retinochoroidal tissues from the posterior eyecups were extracted into soluble fractions. The soluble fractions were then either (A) directly separated by 2-dimensional gel electrophoresis or (B) immunoprecipitated for F95 reactive species and then separated by 2-dimensional gel electrophoresis. The protein blots from these analysis were then probed for (A) total GFAP or (B) citrullinated GFAP (CGTF-1221 antibody). The digital images were then overlaid (C) to compare different GFAP species (red) with those that contained citrullinated species (green).

APPENDIX 3. GLIAL SPROUTS EMERGING IN THE VITREOUS AFTER ALKALI INJURY.

To access the data, click or select the words "Appendix 3." Mouse eyes were either left uninjured or injured and left to recover for 3 days. Eyes were then examined by immunohistochemistry for GFAP (A-B) or vimentin (C-D) staining and DAPI was employed to stain nuclei. (Scale bar=70 µm)

APPENDIX 4: CO-LOCALIZATION OF CITRULLINATION ON GFAP FILAMENTS AT 3 H

To access the data, click or select the words "Appendix 4." Plane-by-Plane Confocal Imaging of 3 Hour Injured eyes Immunostained for F95 (green), GFAP (red), DAPI (blue). Confocal z-stacks were obtained on a Zeiss 780 Confocal microscope at 63X. Individual planes were then increased in brightness to the same level in Lightroom. Images were re-assembled as a .mov at 0.5 s per focal plane. Images encompass planes containing GFAP staining to highlight co-localization with citrullinated species over the length of glial processes.

APPENDIX 5: CO-LOCALIZATION OF CITRULLINATION ON GFAP FILAMENTS AT 3 DAYS

To access the data, click or select the words "Appendix 5." Plane-by-Plane Confocal Imaging of 3 Day Injured eyes Immunostained for F95 (green), GFAP (red), DAPI (blue). Confocal z-stacks were obtained on a Zeiss 780 Confocal microscope at 63X. Individual planes were then increased in brightness to the same level in Lightroom. Images were re-assembled as a .mov at 0.5 s per focal plane. Images encompass planes containing GFAP staining to highlight co-localization with citrullinated species over the length of glial processes.

APPENDIX 6: CO-LOCALIZATION OF CITRULLINATION ON VIMENTIN FILAMENTS AT 3 H

To access the data, click or select the words "Appendix 6." Plane-by-Plane Confocal Imaging of 3 Hour Injured eyes Immunostained for F95 (green), vimentin (red), DAPI (blue). Confocal z-stacks were obtained on a Zeiss 780 Confocal microscope at 63X. Individual planes were then increased in brightness to the same level in Lightroom. Images were re-assembled as a .mov at 0.5 s per focal plane. Images encompass planes containing vimentin staining to highlight co-localization with citrullinated species over the length of individual glial processes.

APPENDIX 7: CO-LOCALIZATION OF CITRULLINATION ON VIMENTIN FILAMENTS AT 3 DAYS

To access the data, click or select the words "Appendix 7." Plane-by-Plane Confocal Imaging of 3 Day Injured eyes Immunostained for F95 (green), vimentin (red), DAPI (blue). Confocal z-stacks were obtained on a Zeiss 780 Confocal microscope at 63X. Individual planes were then increased in brightness to the same level in Lightroom. Images were re-assembled as a .mov at 0.5 s per focal plane. Images encompass planes containing vimentin staining to highlight co-localization with citrullinated species over the length of glial processes.

APPENDIX 8. RESPONSE OF CITRULLINATED PROTEINS TO CL−AMIDINE DOSAGE IN POSTERIOR EYECUP EXPLANT CULTURE.

To access the data, click or select the words "Appendix 8." Mouse eyes were injured and left to recover for 7 days in vivo. On day 7, eyes were enucleated and intact posterior eyecups were placed into culture with vehicle DMSO (lane 1) or different concentrations of Cl−amidine (lanes 2–4) for 3 days. Retinochoroidal tissues from the posterior eyecups were extracted and soluble fractions analyzed by western blotting for citrullinated proteins (F95 antibody), and subsequently, for β-tubulin on the same membrane for loading control.

ACKNOWLEDGMENTS

This work was supported in part by funding from the National Eye Institute/NIH grant R01EY016782 and from the John A. and Florence Mattern Solomon Endowed Chair

in Vision Biology and Eye Diseases. Conflicts of Interest: The funders had no role in study design, data collection and analysis, decision to publish, or preparation of the manuscript. Royce Mohan is one of the inventors on US Patent 8,283,323.

REFERENCES

1. Pekny M, Pekna M. Astrocyte reactivity and reactive astrogliosis: costs and benefits. Physiol Rev 2014; 94:1077-98. [PMID: 25287860].
2. Sofroniew MV. Molecular dissection of reactive astrogliosis and glial scar formation. Trends Neurosci 2009; 32:638-47. [PMID: 19782411].
3. Bringmann A, Wiedemann P. Müller glial cells in retinal disease. Ophthalmologica 2012; 227:1-19. [PMID: 21921569].
4. Petrukhin K. New therapeutic targets in atrophic age-related macular degeneration. Expert Opin Ther Targets 2007; 11:625-39. [PMID: 17465722].
5. Wu KH, Madigan MC, Billson FA, Penfold PL. Differential expression of GFAP in early v late AMD: a quantitative analysis. Br J Ophthalmol 2003; 87:1159-66. [PMID: 12928288].
6. Pekny M, Wilhelmsson U, Pekna M. The dual role of astrocyte activation and reactive gliosis. Neurosci Lett 2014; 565:30-8. [PMID: 24406153].
7. Joshi M, Agrawal S, Christoforidis JB. Inflammatory mechanisms of idiopathic epiretinal membrane formation. Mediators Inflamm 2013; 192582:[PMID: 24324293].
8. Lewis GP, Fisher SK. Müller cell outgrowth after retinal detachment: association with cone photoreceptors. Invest Ophthalmol Vis Sci 2000; 41:1542-5. [PMID: 10798674].
9. Gandorfer A, Haritoglou C, Scheler R, Schumann R, Zhao F, Kampik A. Residual cellular proliferation on the internal limiting membrane in macular pucker surgery. Retina 2012; 32:477-85. [PMID: 22068175].
10. Pekny M, Johansson CB, Eliasson C, Stakeberg J, Wallén A, Perlmann T, Lendahl U, Betsholtz C, Berthold CH, Frisén J. Abnormal reaction to central nervous system injury in mice lacking glial fibrillary acidic protein and vimentin. J Cell Biol 1999; 145:503-14. [PMID: 10225952].
11. Lundkvist A, Reichenbach A, Betsholtz C, Carmeliet P, Wolburg H, Pekny M. Under stress, the absence of intermediate filaments from Müller cells in the retina has structural and functional consequences. J Cell Sci 2004; 117:3481-8. [PMID: 15226376].
12. Ralton JE, Lu X, Hutcheson AM, Quinlan RA. Identification of two N-terminal non-alphα-helical domain motifs important in the assembly of glial fibrillary acidic protein. J Cell Sci 1994; 107:1935-48. [PMID: 7983160].
13. Inagaki M, Nishi Y, Nishizawa K, Matsuyama M, Sato C. Site-specific phosphorylation induces disassembly of vimentin filaments in vitro. Nature 1987; 328:649-52. [PMID: 3039376].
14. Inagaki M, Takahara H, Nishi Y, Sugawara K, Sato C. Ca2+-dependent deimination-induced disassembly of intermediate filaments involves specific modification of the N-terminal head domain. J Biol Chem 1989; 264:18119-27. [PMID: 2808368].
15. Korolainen MA, Auriola S, Nyman TA, Alafuzoff I, Pirttilä T. Proteomic analysis of glial fibrillary acidic protein in Alzheimer's disease and aging brain. Neurobiol Dis 2005; 20:858-70. [PMID: 15979880].
16. Nicholas AP, King JL, Sambandam T, Echols JD, Gupta KB, McInnis C, Whitaker JN. Immunohistochemical localization of citrullinated proteins in adult rat brain. J Comp Neurol 2003; 459:251-66. [PMID: 12655508].
17. Nicholas AP, Sambandam T, Echols JD, Barnum SR. Expression of citrullinated proteins in murine experimental autoimmune encephalomyelitis. J Comp Neurol 2005; 486:254-66. [PMID: 15844173].
18. Wang S, Wang Y. Peptidylarginine deiminases in citrullination, gene regulation, health and pathogenesis. Biochim Biophys Acta 2013; 1829:1126-35. [PMID: 23860259].
19. Ishigami A, Ohsawa T, Hiratsuka M, Taguchi H, Kobayashi S, Saito Y, Murayama S, Asaga H, Toda T, Kimura N, Maruyama N. Abnormal accumulation of citrullinate proteins catalyzed by peptidylarginine deiminase in hippocampal extracts from patients with Alzheimer's disease. J Neurosci Res 2005; 80:120-8. [PMID: 15704193].
20. Nicholas AP, Sambandam T, Echols JD, Tourtellotte WW. Increased citrullinated glial fibrillary acidic protein in secondary progressive multiple sclerosis. J Comp Neurol 2004; 473:128-36. [PMID: 15067723].
21. Moscarello MA, Lei H, Mastronardi FG, Winer S, Tsui H, Li Z, Ackerley C, Zhang L, Raijmakers R, Wood DD. Inhibition of peptidyl-arginine deiminases reverses protein-hypercitrullination and disease in mouse models of multiple sclerosis. Dis Model Mech 2013; 6:467-78. [PMID: 23118341].
22. Bonilha VL, Shadrach KG, Rayborn ME, Li Y, Pauer GJ, Hagstrom SA, Bhattacharya SK, Hollyfield JG. Retinal deimination and PAD2 levels in retinas from donors with age-related macular degeneration (AMD). Exp Eye Res 2013; 111:71-8. [PMID: 23562679].
23. Bhattacharya SK, Crabb JS, Bonilha VL, Gu X, Takahara H, Crabb JW. Proteomics implicates peptidyl arginine deiminase 2 and optic nerve citrullination in glaucoma pathogenesis. Invest Ophthalmol Vis Sci 2006; 47:2508-14. [PMID: 16723463].
24. Algeciras ME, Takahara H, Bhattacharya SK. Mechanical stretching elevates peptidyl arginine deiminase 2 expression in astrocytes. Curr Eye Res 2008; 33:994-1001. [PMID: 19085382].
25. Powell C, Grant AR, Cornblath E, Goldman D. Analysis of DNA methylation reveals a partial reprogramming of the Müller glia genome during retina regeneration. Proc Natl Acad Sci USA 2013; 110:19814-9. [PMID: 24248357].

26. Galan A, Dergham P, Escoll P, de-la-Hera A, D'Onofrio PM, Magharious MM, Koeberle PD, Frade JM, Saragovi HU. Neuronal injury external to the retina rapidly activates retinal glia, followed by elevation of markers for cell cycle re-entry and death in retinal ganglion cells. PLoS ONE 2014; 9:e101349-[PMID: 24983470].

27. Dyer MA, Cepko CL. Control of Müller glial cell proliferation and activation following retinal injury. Nat Neurosci 2000; 3:873-80. [PMID: 10966617].

28. Tackenberg MA, Tucker BA, Swift JS, Jiang C, Redenti S, Greenberg KP, Flannery JG, Reichenbach A, Young MJ. Müller cell activation, proliferation and migration following laser injury. Mol Vis 2009; 15:1886-96. [PMID: 19768129].

29. Lewis GP, Chapin EA, Luna G, Linberg KA, Fisher SK. The fate of Müller's glia following experimental retinal detachment: nuclear migration, cell division, and subretinal glial scar formation. Mol Vis 2010; 16:1361-72. [PMID: 20664798].

30. Lange S, Gögel S, Leung KY, Vernay B, Nicholas AP, Causey CP, Thompson PR, Greene ND, Ferretti P. Protein deiminases: new players in the developmentally regulated loss of neural regenerative ability. Dev Biol 2011; 355:205-14. [PMID: 21539830].

31. Traub P, Vorgias CE. Differential effect of arginine modification with 1,2-cyclohexanedione on the capacity of vimentin and desmin to assemble into intermediate filaments and to bind to nucleic acids. J Cell Sci 1984; 65:1-20. [PMID: 6325477].

32. Bargagna-Mohan P, Paranthan RR, Hamza A, Dimova N, Trucchi B, Srinivasan C, Elliott GI, Zhan CG, Lau DL, Zhu H, Kasahara K, Inagaki M, Cambi F, Mohan R. Withaferin A targets intermediate filaments glial fibrillary acidic protein and vimentin in a model of retinal gliosis. J Biol Chem 2010; 285:7657-69. [PMID: 20048155].

33. Paranthan RR, Bargagna-Mohan P, Lau DL, Mohan R. A robust model for simultaneously inducing corneal neovascularization and retinal gliosis in the mouse eye. Mol Vis 2011; 17:1901-8. [PMID: 21850164].

34. Mohan R, Hammers HJ, Bargagna-Mohan P, Zhan XH, Herbstritt CJ, Ruiz A, Zhang L, Hanson AD, Conner BP, Rougas J, Pribluda VS. Withaferin A is a potent inhibitor of angiogenesis. Angiogenesis 2004; 7:115-22. [PMID: 15516832].

35. Bargagna-Mohan P, Hamza A, Kim YE, Khuan Abby Ho Y, Mor-Vaknin N, Wendschlag N, Liu J, Evans RM, Markovitz DM, Zhan CG, Kim KB, Mohan R. The tumor inhibitor and antiangiogenic agent withaferin A targets the intermediate filament protein vimentin. Chem Biol 2007; 14:623-34. [PMID: 17584610].

36. Bargagna-Mohan P, Paranthan RR, Hamza A, Zhan CG, Lee DM, Kim KB, Lau DL, Srinivasan C, Nakayama K, Nakayama KI, Herrmann H, Mohan R. Corneal antifibrotic switch identified in genetic and pharmacological deficiency of vimentin. J Biol Chem 2012; 287:989-1006. [PMID: 22117063].

37. Mohan R, Bargagna-Mohan P. The use of withaferin A to study intermediate filaments. Methods Enzymol 2016; 568:187-218. [PMID: 26795472].

38. Miyazaki K, Okada Y, Yamanaka O, Kitano A, Ikeda K, Kon S, Uede T, Rittling SR, Denhardt DT, Kao WW, Saika S. Corneal wound healing in an osteopontin-deficient mouse. Invest Ophthalmol Vis Sci 2008; 49:1367-75. [PMID: 18385052].

39. Tuft SJ, Shortt AJ. Surgical rehabilitation following severe ocular burns. Eye (Lond) 2009; 23:1966-71. [PMID: 19169226].

40. Ishigami A, Masutomi H, Handa S, Nakamura M, Nakaya S, Uchida Y, Saito Y, Murayama S, Jang B, Jeon YC, Choi EK, Kim YS, Kasahara Y, Maruyama N, Toda T. Mass spectrometric identification of citrullination sites and immunohistochemical detection of citrullinated glial fibrillary acidic protein in Alzheimer's disease brains. J Neurosci Res 2015; 93:1664-74. [PMID: 26190193].

41. Perlson E, Hanz S, Ben-Yaakov K, Segal-Ruder Y, Seger R, Fainzilber M. Vimentin-dependent spatial translocation of an activated MAP kinase in injured nerve. Neuron 2005; 45:715-26. [PMID: 15748847].

42. Bargagna-Mohan P, Lei L, Thompson A, Shaw C, Kasahara K, Inagaki M, Mohan R. Vimentin Phosphorylation Underlies Myofibroblast Sensitivity to Withaferin A In Vitro and during Corneal Fibrosis. PLoS ONE 2015; 10:e0133399-[PMID: 26186445].

43. Menko AS, Bleaken BM, Libowitz AA, Zhang L, Stepp MA, Walker JL. A central role for vimentin in regulating repair function during healing of the lens epithelium. Mol Biol Cell 2014; 25:776-90. [PMID: 24478454].

44. Helfand BT, Mendez MG, Murthy SN, Shumaker DK, Grin B, Mahammad S, Aebi U, Wedig T, Wu YI, Hahn KM, Inagaki M, Herrmann H, Goldman RD. Vimentin organization modulates the formation of lamellipodia. Mol Biol Cell 2011; 22:1274-89. [PMID: 21346197].

45. Luna G, Lewis GP, Banna CD, Skalli O, Fisher SK. Expression profiles of nestin and synemin in reactive astrocytes and Müller cells following retinal injury: a comparison with glial fibrillary acidic protein and vimentin. Mol Vis 2010; 16:2511-23. [PMID: 21139996].

46. Cade F, Paschalis EI, Regatieri CV, Vavvas DG, Dana R, Dohlman CH. Alkali burn to the eye: protection using TNF-α inhibition. Cornea 2014; 33:382-9. [PMID: 24488127].

47. Herskowitz JH, Seyfried NT, Duong DM, Xia Q, Rees HD, Gearing M, Peng J, Lah JJ, Levey AI. Phosphoproteomic analysis reveals site-specific changes in GFAP and NDRG2 phosphorylation in frontotemporal lobar degeneration. J Proteome Res 2010; 9:6368-79. [PMID: 20886841].

48. Sambandam T, Belousova M, Accaviti-Loper MA, Blanquicett C, Guercello V, Raijmakers R, Nicholas AP. Increased peptidylarginine deiminase type II in hypoxic astrocytes. Biochem Biophys Res Commun 2004; 325:1324-9. [PMID: 15555572].

49. Bargagna-Mohan P, Deokule SP, Thompson K, Wizeman J, Srinivasan C, Vooturi S, Kompella UB, Mohan R. Withaferin A effectively targets soluble vimentin in the glaucoma filtration surgical model of fibrosis. PLoS ONE 2013; 8:e63881-[PMID: 23667686].

50. Chumanevich AA, Causey CP, Knuckley BA, Jones JE, Poudyal D, Chumanevich AP, Davis T, Matesic LE, Thompson PR, Hofseth LJ. Suppression of colitis in mice by Cl-amidine: a novel peptidylarginine deiminase inhibitor. Am J Physiol Gastrointest Liver Physiol 2011; 300:G929-38. [PMID: 21415415].

51. Edwards MM, McLeod DS, Bhutto IA, Villalonga MB, Seddon JM, Lutty GA. Idiopathic preretinal glia in aging and age-related macular degeneration. Exp Eye Res 2015; •••:S0014-4835. .

52. Puro DG. Stretch-activated channels in human retinal Müller cells. Glia 1991; 4:456-60. [PMID: 1718863].

53. Liu B, Hunter DJ, Rooker S, Chan A, Paulus YM, Leucht P, Nusse Y, Nomoto H, Helms JA. Wnt signaling promotes Müller cell proliferation and survival after injury. Invest Ophthalmol Vis Sci 2013; 54:444-53. [PMID: 23154457].

54. Giani A, Thanos A, Roh MI, Connolly E, Trichonas G, Kim I, Gragoudas E, Vavvas D, Miller JW. Invest Ophthalmol Vis Sci 2011; 52:3880-7. [PMID: 21296820].

55. Bhattacharya SK, Bhat MB, Takahara H. Modulation of peptidyl arginine deiminase 2 and implication for neurodegeneration. Curr Eye Res 2006; 31:1063-71. [PMID: 17169845].

56. Lin MP, Ekşioğlu Ü, Mudumbai RC, Slabaugh MA, Chen PP. Glaucoma in patients with ocular chemical burns. Am J Ophthalmol 2012; 154:481-5. [PMID: 22633350].

57. Chirivi RGS, Jenniskens GJ, Raats JMH. Anti-Citrullinated Protein Antibodies as Novel Therapeutic Drugs in Rheumatoid Arthritis. J Clin Cell Immunol. 2013.

Articles are provided courtesy of Emory University and the Zhongshan Ophthalmic Center, Sun Yat-sen University, P.R. China. The print version of this article was created on 26 September 2016. This reflects all typographical corrections and errata to the article through that date. Details of any changes may be found in the online version of the article.